ACS APPLIED MATERIALS & INTERFACES

Research Article

www.acsami.org

Moisture Condensation Behavior of Hierarchically Carbon Nanotube-Grafted Carbon Nanofibers

Kyu-Min Park,[†] Byoung-Sun Lee,[†] Ji Ho Youk,[‡] Jinyong Lee,[§] and Woong-Reol Yu*[,†]

[†]Department of Materials Science and Engineering and Research Institute of Advanced Materials, Seoul National University, 599 Gwanangro, Gwanak-gu, Seoul, 151-742, Republic of Korea

[‡]Department of Advanced Fiber Engineering, Inha University, 100 Inharo, Nam-gu, Incheon, 402-751, Republic of Korea

[§]High Temperature Composite Materials Group, Agency for Defense Development, 111 Sunam-dong, Yuseong-gu, Daejeon, 305-600, Republic of Korea

ABSTRACT: Hierarchical micro/nanosurfaces with nanoscale roughness on microscale uneven substrates have been the subject of much recent research interest because of phenomena such as superhydrophobicity. However, an understanding of the effect of the difference in the scale of the hierarchical entities, i.e., nanoscale roughness on microscale uneven substrates as opposed to nanoscale roughness on (a larger) nanoscale uneven surface, is still lacking. In this study, we investigated the effect of the difference in scale between the nano- and microscale features. We fabricated carbon nanotube-grafted carbon nanofibers (CNFs) by dispersing a catalyst precursor in poly (acrylonitrile) (PAN) solution, electrospinning the PAN/catalyst precursor solution, carbonization of electrospun PAN nanofibers, and direct growth of carbon nanotubes (CNTs) on the CNFs. We investigated the relationships between the catalyst concentrations, the size of catalyst nanoparticles on CNFs, and the sizes of CNFs and CNTs. Interestingly, the hydrophobic behavior of micro/nano and nano/nano hierarchical surfaces with water droplets was similar; however a significant difference in the water condensation behavior was observed. Water condensed into smaller droplets on the nano/nano hierarchical surface, causing it to dry much faster.

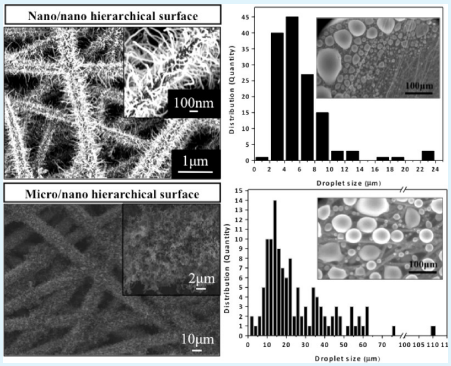

KEYWORDS: *carbon nanotubes, carbon nanofibers, hierarchical surface, scale difference, rapid dry, moisture*

1. INTRODUCTION

The surface modification of materials, including changes in the surface roughness,[1] hydrophobicity,[2] surface charge,[3] surface energy,[4] biocompatibility,[3,5] and surface reactivity,[6] has become an increasingly popular method to study multifunctionalities of materials, where a desired functionality can be achieved without incurring large expenses and long lead times for developing new functional materials. Control over the hydrophobicity is one of the most useful aspects of micro/nano hierarchical patterns, with applications in areas including oil−water separation, friction reduction, anticontamination, and self-cleaning.[7−10]

The hydrophobicity of solids is determined by the surface free energy and geometrical roughness.[11−13] Since a reduction in the surface free energy increases the hydrophobicity, a number of approaches have been employed to reduce the surface energy of materials and thus enhance their hydrophobicity, including direct exposure to F_2 gas,[14] fluorine-containing electrical discharges,[15] and sputter deposition from a poly(tetrafluorethylene) (PTFE) target.[16] Increasing the roughness of a surface can also enhance the hydrophobicity of a material. Roughness can be introduced on surfaces using various methods, including chemical vapor deposition (CVD),[17,18] sol−gel processing,[19] electrospinning,[20,21] self-assembly,[22−25] lithographic patterning,[26] and vertical alignment of nanotubes or nanofibers.[27,28]

Previous studies in inducing hydrophobicity can be broadly classified into two categories: (1) introduction of microscale roughness onto substrates together with hydrophobic coatings, including fluorinated surfaces[29,30] and (2) hierarchical introduction of nanoscale roughness on a microscale uneven surface.[31,32] The two methods share a common feature of microscale unevenness in the substrate. Microscale unevenness is known to repel large water droplets effectively; however, it is not as effective with small water droplets trapped between micropillars.[33] Therefore, the scale of the surface features is an important factor in determining hydrophobicity, in particular the droplet-size dependence of the hydrophobicity. However, the effect of the scale of the surface features has not yet been systematically investigated. We investigated the effect of the relative scales of the patterns by fabricating a hierarchical surface consisting of nanoscale features patterned onto substrates with larger nanoscale to microscale unevenness.

Electrospinning is a cost-effective and versatile method to prepare substrates with nanoscale unevenness, on which smaller nanoscale unevenness can be introduced.[34−36] In this study, poly (acrylonitrile) (PAN)/$Fe(Acc)_3$ solutions were electrospun into

Received: August 11, 2013
Accepted: October 11, 2013
Published: October 11, 2013

nanofibers, followed by carbonization, resulting in carbon nanofibers (CNFs) and catalysts nanoparticles were formed on the surface and inside the body of CNFs. Carbon nanotubes (CNTs) were then grown directly on the CNF surface using CVD, introducing smaller nanoscale roughness on the larger nanoscale uneven substrate. This material, termed here CNT-grafted-CNF, was investigated, focusing on the fabrication method and surface behavior.

2. EXPERIMENTAL SECTION

2.1. Materials. Poly(acrylonitrile) (PAN, M_w = 200 000 g/mol, Misui chemical) and Iron(III) acetylacetonate ($Fe(Acc)_3$) were dissolved in *N*,*N*-dimethylformamide (DMF, Sigma-Aldrich). To uniformly disperse Fe ions in the solution, $Fe(Acc)_3$ was dissolved in 16 mL of DMF and heated to 90 °C, followed by magnetic stirring for 2 h. Three kinds of solutions were prepared by varying the amount of $Fe(Acc)_3$, so that 0.2, 0.4, and 0.6 g were dissolved in the DMF. PAN (4 g) was then dissolved in each solution and stirred for 5 h. The solutions were then cooled to room temperature.

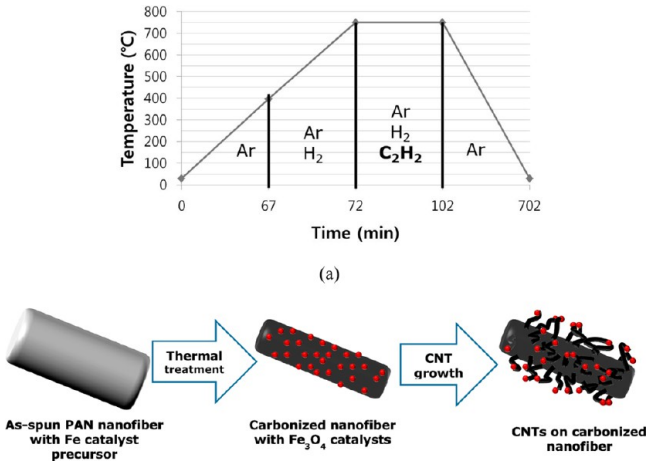

Figure 1. Schematic diagrams illustrating (a) CVD process and (b) morphological change of nanofibers.

2.2. Electrospinning and CVD Processes. PAN nanofibers containing Fe were manufactured by electrospinning using a direct current voltage of 15 kV, a flow rate of 0.5 mL/h, and a tip-to-collector separation of 10 cm. Thermal treatment processes for stabilization and carbonization were applied to the PAN nanofibers. Stabilization occurred in the temperature range 270−300 °C in an air atmosphere for 1 h, and subsequent carbonization was carried out at 1000 °C in an N_2 atmosphere for 1 h. The temperature was raised at a rate of 10 °C/min. During the thermal treatment, PAN nanofibers were converted into CNFs containing Fe nanoparticles, which acted as catalysts to grow CNTs in the following CVD process.

The CNTs were then synthesized on the carbon fibers using CVD. Ar (500 sccm), H_2 (50 sccm), and C_2H_2 (50 sccm) were used as the carrier gas, reduction agent, and carbon sources, respectively. The furnace temperature and sequential gas injections were programed as shown in Figure 1a. The morphological change of the CNFs during the CVD process is illustrated schematically in Figure 1b.

2.3. Morphologies and Surface Behavior of CNFs. The morphologies of CNFs and CNT-grafted-CNFs were investigated using field-emission scanning electron microscopy (FE-SEM) (SUPRA 55VP, Carl Zeiss, operating at 2.00 kV) and high-resolution transmission electron microscopy (HR-TEM) (JEM-3000F). The microstructures were characterized using X-ray diffraction (XRD) (New D8 Advance).

The hydrophobicity of both the CNFs and CNT-grafted-CNFs was characterized by measuring the contact angle (CA) with a 30-μm-diameter water droplet at room temperature using a dynamic CA analyzer (Phoenix 150, S.E.O.). In addition, the water condensation behavior was investigated using an environmental scanning electron microscope (ESEM) (XL-30 FEG). After holding the samples within the ESEM, moisture was introduced into the ESEM chamber, which was maintained at 2 °C, and the pressure was increased to 4.6−5 Torr, forming fine water droplets on the material surfaces. The morphology of the water droplets was captured using the ESEM and analyzed by focusing on the size distribution of individual water droplets formed on the substrate. The size of the water droplets depends on the substrate

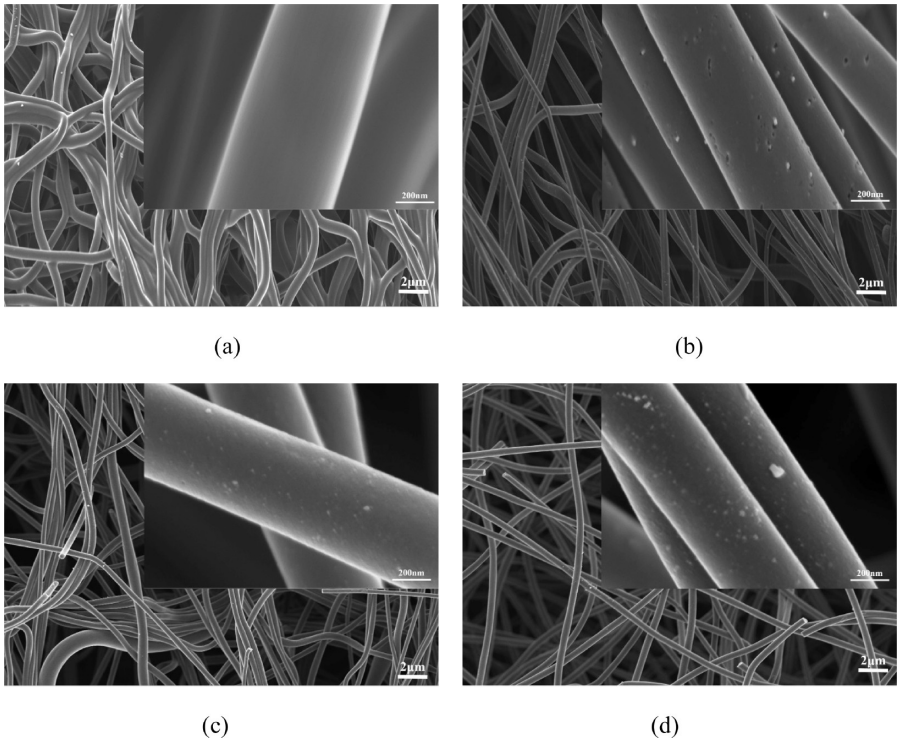

Figure 2. SEM images of the CNFs prepared from different $Fe(Acc)_3$ concentrations: (a) 0, (b) 1, (c) 2, and (d) 3 wt %.

structure; therefore, this experiment was designed to characterize the effect of the scale of the substrate surface roughness on the size of the droplets and, hence, the resulting drying rate of the moisture.

3. RESULTS AND DISCUSSION

3.1. Morphologies of CNT-grafted-CNFs. The morphologies of the CNFs, prepared by electrospinning and subsequent thermal treatment for stabilization and carbonization, were investigated using FE-SEM (Figure 2). Nanoparticles can be clearly seen on the surfaces of the CNFs. XRD was used to identify these nanoparticles, as shown in Figure 3. CNFs prepared from PAN solution without $Fe(Acc)_3$ showed two diffraction peaks at (002) and (10*l*), which is typical for carbon crystals, whereas CNFs prepared from PAN solution containing $Fe(Acc)_3$ exhibited six additional diffraction peaks at (110), (220), (311), (208), (511), and (440). These diffraction peaks are attributable to Fe_3O_4 crystals (from JCPDS 85-1435). The Fe_3O_4 nanoparticles were formed during heat treatment at 1000 °C and originated from $Fe(Acc)_3$ added in the PAN solution (see section 2.1). Fe atoms diffused through the porous structure of CNFs during stabilization and carbonization of PAN and then aggregated into Fe_3O_4 nanoparticles.[37] In addition to the CNF surface, Fe_3O_4 nanoparticles were also observed inside the CNFs. Figure 4 shows that several Fe_3O_4 nanoparticles formed inside the CNFs; more graphitic layers appeared around these particles, implying that the carbon crystal developed more around the Fe_3O_4 nanoparticles than any other part of the CNFs. This is

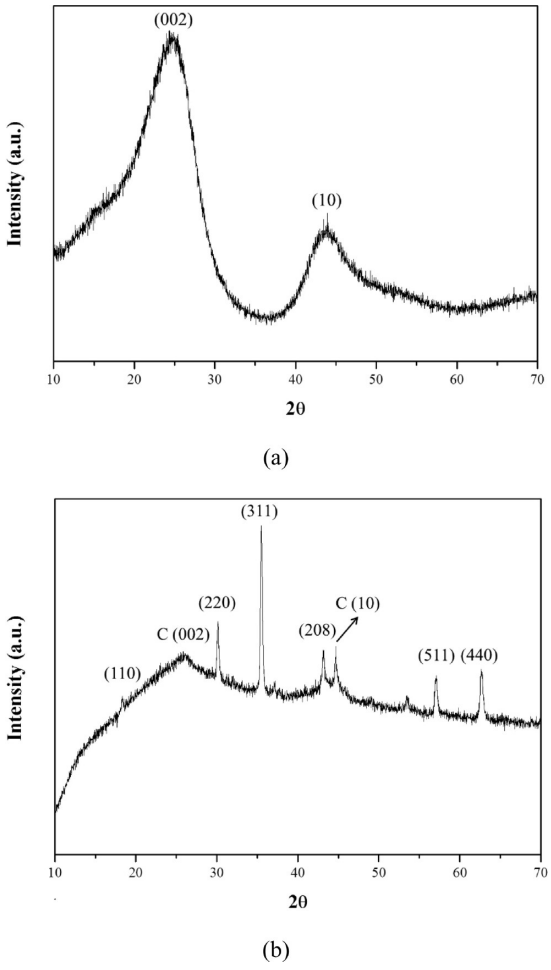

Figure 3. XRD pattern of the CNFs (a) without and (b) with Fe catalyst. CNFs prepared without $Fe(Acc)_3$ showed peaks at (002) and (10l), whereas CNFs with $Fe(Acc)_3$ showed additional six diffraction peaks at (110), (220), (311), (208), (511), and (440).

Table 1. Sizes of Fe Catalyst Nanoparticles and CNFs According to $Fe(Acc)_3$ Concentration

diameter	Fe 1 wt %	Fe 2 wt %	Fe 3 wt %
catalyst particle (nm)	16.3 (±4.9)	20.1 (±5.7)	23.3 (±6.8)
nanofiber (nm)	448.9 (±79.6)	373.7 (±64.8)	359.9 (±58.9)

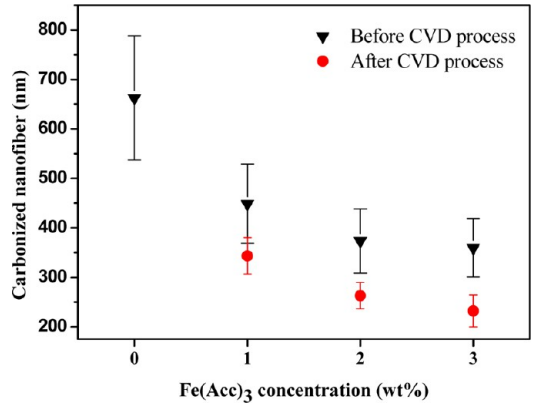

Figure 5. Changes in the diameter of CNFs depending on $Fe(Acc)_3$ concentration. Note that the diameters of CNFs were also characterized after CVD growth of the CNTs.

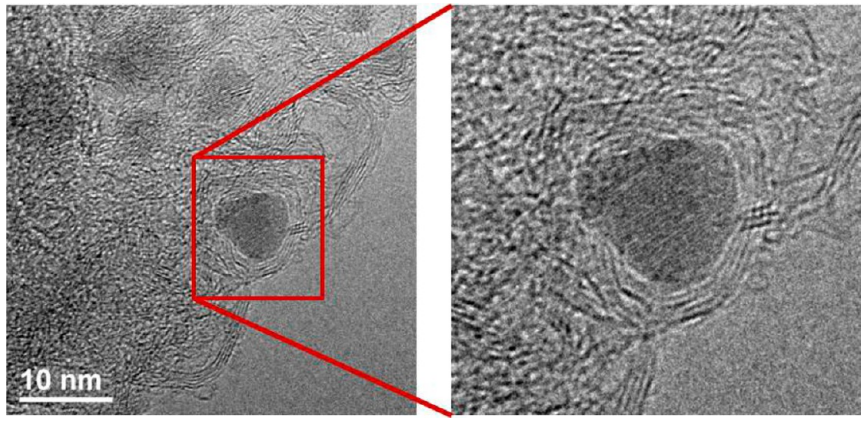

Figure 4. TEM image of Fe catalyst inside CNFs. The graphene layers were aligned around the catalyst nanoparticle, suggesting that catalytic graphitization occurred during the heat treatment.

dx.doi.org/10.1021/am403348q | ACS Appl. Mater. Interfaces 2013, 5, 11115−11122

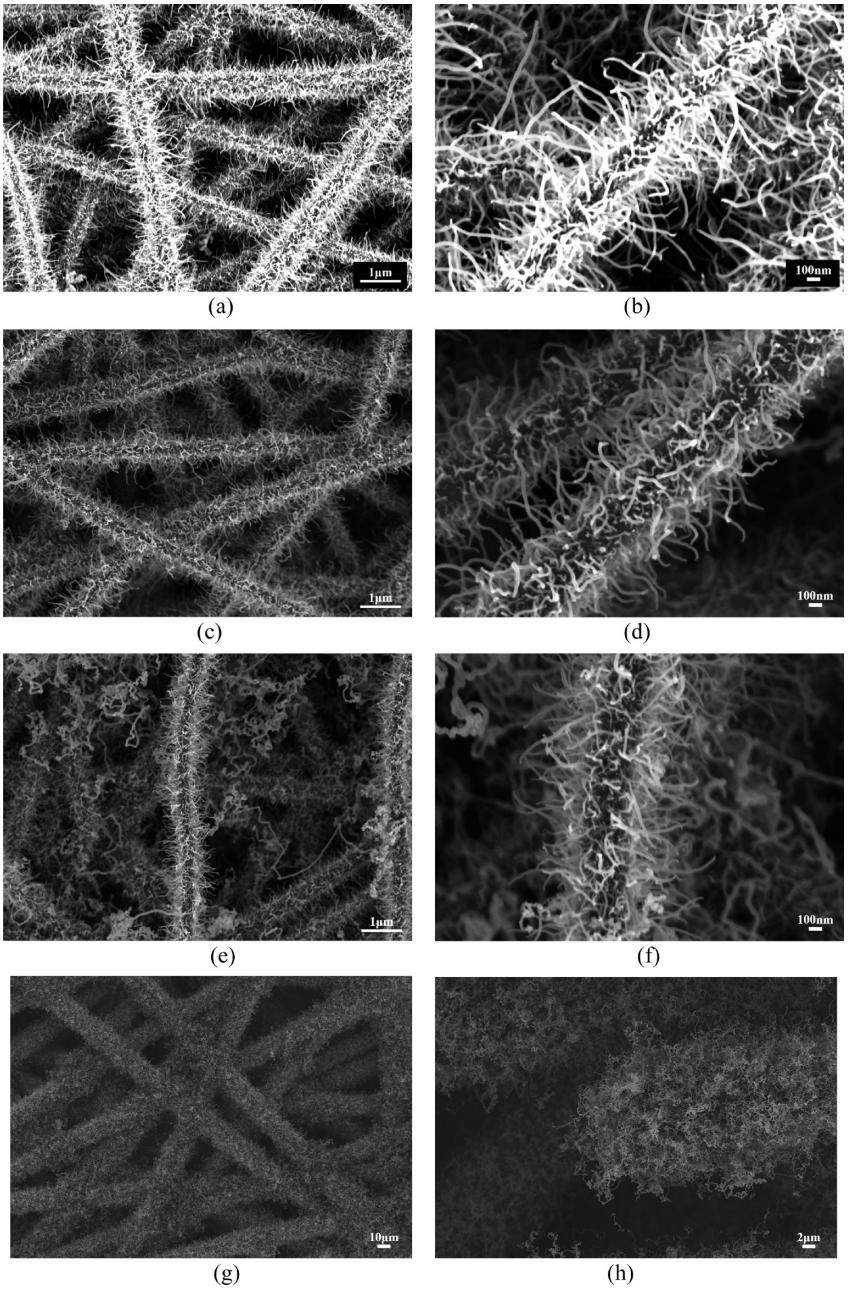

Figure 6. Morphologies of CNTs grown on CNFs and carbon papers. (a) $Fe(Acc)_3$ 1 wt %, (c) $Fe(Acc)_3$ 2 wt %, (e) $Fe(Acc)_3$ 3 wt %, (b, d, and f) magnified images of parts a, c, and e, respectively, (g) CNTs on carbon papers, (h) magnified image of part g.

attributable to catalytic graphitization by metal oxides; the formation of carbon crystals is facilitated around metal oxide catalysts to reduce the total energy (increased by the metal catalyst).[38−40]

The size of the Fe_3O_4 nanoparticles varied depending on the $Fe(Acc)_3$ concentration and ranged from 16 to 23 nm. Larger Fe_3O_4 nanoparticles occurred on an increased concentration of $Fe(Acc)_3$ (see Table 1), because the coalescence of Fe atoms into nanoparticles is proportional to Fe concentration. Larger catalyst nanoparticles will grow larger CNTs during the subsequent CVD process, making the surface rougher, as discussed later. The $Fe(Acc)_3$ concentration affected the diameter of the CNFs, as compared in Table 1 (see also Figures 2 and 5). The diameter of the CNFs decreased with increasing $Fe(Acc)_3$ concentration; this can be explained by two factors. First, catalytic graphitization occurred around metal catalyst particles, i.e., larger Fe_3O_4 nanoparticles led to more catalytic graphitization (equivalently more carbon crystals), resulting in a significant reduction of the CNF volume and thus a decrease in the diameter. Second, the size of the precursor nanofibers, i.e., the size of as-spun PAN nanofibers, was influenced by the $Fe(Acc)_3$ concentration. The diameter of as-spun PAN nanofibers decreased as the $Fe(Acc)_3$ concentration increased, which is attributable to the reduced electrical conductivity of the PAN/$Fe(Acc)_3$ solution, inducing more charge build-up on the Taylor cone and thus greater electrical pulling during electrospinning.[41]

Figure 6 shows SEM images of CNT-grafted-CNFs (and CNT-grafted carbon papers), demonstrating that CNTs were uniformly grown on the CNFs surfaces. The Fe nanoparticles acted as a catalyst for CNT growth during the thermal CVD

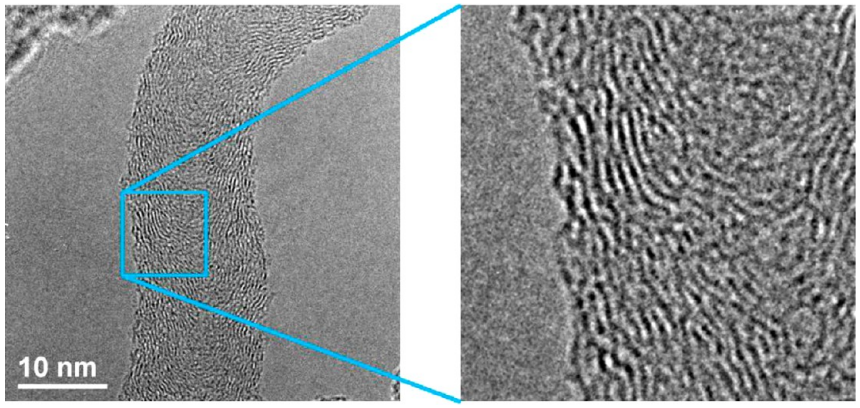

Figure 7. TEM image of a CNT grown on a CNF.

process. Note that CNTs were grown on CNFs regardless of location (i.e., whether the CNFs were on the inside of the surface). This uniform CNT growth was achieved by controlling the concentrations of the carbon sources and the reaction time between carbon source and catalyst particles. The grown CNTs seem to be well linked to the nanofibers because we could not observe the CNTs separated from the fibers during the following experiments. The CNTs grown on the CNF surface were investigated using TEM to determine their microstructure. As shown in Figure 7, instead of straight walls, bamboo-like or cup-stacked wall structures were observed. These kinds of wall structures have been reported previously.[42,43] Nevertheless, it is clear that Fe_3O_4 particles catalyzed the carbon sources, inducing CNT growth. The length and diameter of the CNTs were also characterized to investigate the effect of the catalyst nanoparticles (see Table 1), in particular the effect of the size of the Fe_3O_4 particles on the CNT morphologies. Larger catalyst particles led to thicker CNTs, as shown in Figure 8. This is related to the

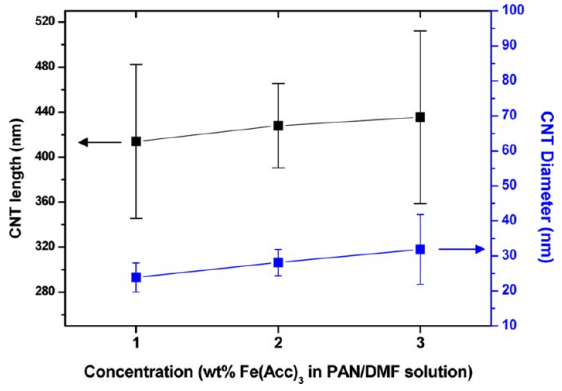

Figure 8. Length and diameters of CNTs grown on CNFs produced as a function of $Fe(Acc)_3$ concentration.

growth mechanism (i.e., the solvation of the carbon vapor in metal clusters and the precipitation of excess carbons into CNTs[44]); thus, if the carbon source is sufficient, the diameter of CNTs is determined by the catalyst size. As for the length of CNTs, it seem to increase as the sizes of the catalyst nanoparticles increase; however, this cannot be concluded from Figure 8 because the standard deviation of CNT length was very large. CNTs are known to grow in tip growth mode on a carbon substrate.[45] In this study, we observed Fe_3O_4 nanoparticles dangling at the top of the CNTs, which is consistent with previous reports. Note that the CNT-grafted-CNFs can be manipulated by magnetic fields owing to the Fe_3O_4 nanoparticles, which were dangled at the top of the CNTs or resided in the CNTs, e.g., a magnetic bar can be used to collect the material from a solution.

3.2. Surface (Hydrophobic) Behavior of CNT-Grafted-CNF Mats. The surface properties of CNT-grafted-CNFs were investigated by carrying out two experiments: CA measurements and moisture condensation observations. Figure 9 shows the shapes of water droplets formed on the surface of the CNT-grafted-CNFs. The water droplet was well wet into the CNF surface without CNTs, and the CA was about 30° (see Figures 9a and 10 for the appearance and CA data, respectively). This observation implies that the surface energy of the CNFs was high enough to overcome the surface tension of the water; i.e., the CNF surface was hydrophilic. A significant change in the CA was observed for CNT-grafted-CNFs. As shown in Figure 9b–d, CNTs played a significant role in the hydrophobic behavior of CNT-grafted-CNFs; the surface became superhydrophobic due to the nanoscale roughness caused by the CNTs. The CA increased to 155° for CNF-grafted-CNFs prepared from an $Fe(Acc)_3$ concentration of 3 wt %. This is not surprising[46] because the hierarchical CNTs increase the surface roughness on the micrometer scale; this balances the surface tension of water droplet and the air trapped in the nanoscale unevenness, preventing water from penetrating into nanosized valleys.

To investigate the effect of the scale of the substrate unevenness, sheets of carbon paper consisting of carbon micro fibers were also treated using the same process conditions used for grafting CNTs onto CNFs, except for the catalyst introduction process. The catalysts were introduced into the carbon paper through solution dipping; i.e., the carbon paper was immersed in $Fe(Acc)_3$ solution (1 wt %). The dimensions of grown CNTs on the carbon paper were about 7.2 μm and 45 nm in length and diameter, respectively. As shown in Figure 9e, the carbon paper without CNTs show hydrophobic behavior with a CA of 121°, whereas CNTs grafted on the carbon paper resulted in superhydrophobic behavior (see Figures 9f and 10). Comparing this result with the aforementioned CNT-grafted-CNFs, the effect of the scale of the substrate unevenness (i.e., nanoscale CNFs and microscale carbon paper) on the hydrophobic behavior appears negligible for the water droplet used in the CA test. However, this water droplet was relatively large, and the hydrophobic behavior of these materials with smaller water droplets was investigated using another method, moisture condensation.

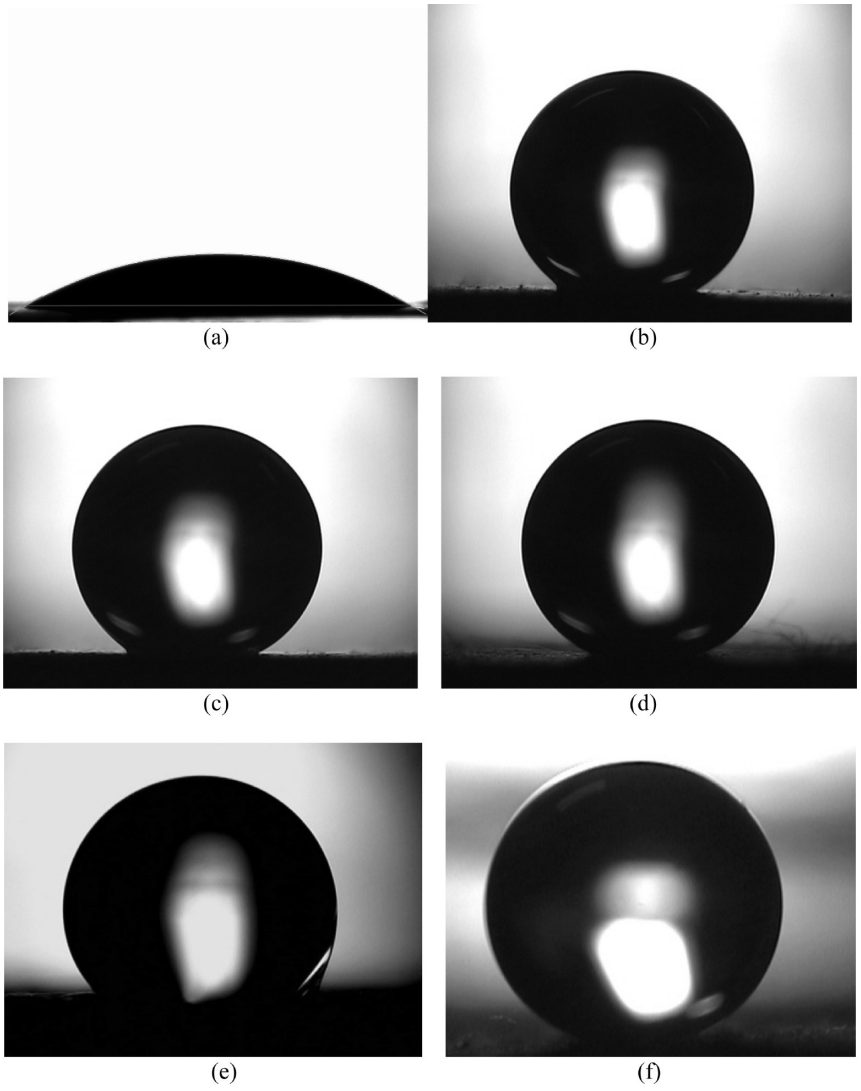

Figure 9. Shapes of water droplets formed on CNT-grafted-CNFs depending on the $Fe(Acc)_3$ concentration: (a) 0, (b) 1, (c) 2, and (d) 3 wt %. For comparison, two more samples were prepared: (e) carbon paper and (f) CNT-grafted carbon paper.

Water vapor can condense into water droplets if the temperature and pressure conditions are appropriate. In this study, water condensation was induced on the CNFs and carbon paper by maintaining a temperature of 2 °C and increasing the pressure from 4.6 to 5 Torr (see Figure 11). CNFs and carbon paper without grafted CNTs are not hydrophobic, as discussed above; Figure 11a and c show that water spread on the substrates. As the moisture condensed into water droplets, they wetted the substrate, resulting in the coalescence of water droplets into a water film. Hydrophobicity of the substrate is a requirement to maintain water droplets condensed from moisture. Due to their superhydrophobic nature, both CNT-grafted-CNFs and carbon paper with grafted CNTs exhibited water droplets on their surfaces, and the droplets did not spread into a film, as shown in Figure 11b and d. However, the sizes of the water droplets were quite different between the two substrates. The size distributions of the water droplets were characterized by measuring the diameters using an ESEM and are shown in Figure 12. The mean diameter of the water droplets was 5 μm on the CNT-grafted-CNFs and 18 μm for on the CNT-grafted carbon paper. The finer the filaments of the substrates (i.e., nanofibers and microfibers), the smaller the water droplets became. This can be explained by considering the hydrophobic surface and the filament size. The carbon papers with grafted CNTs were superhydrophobic; thus, the condensed water droplets remained and became larger as long

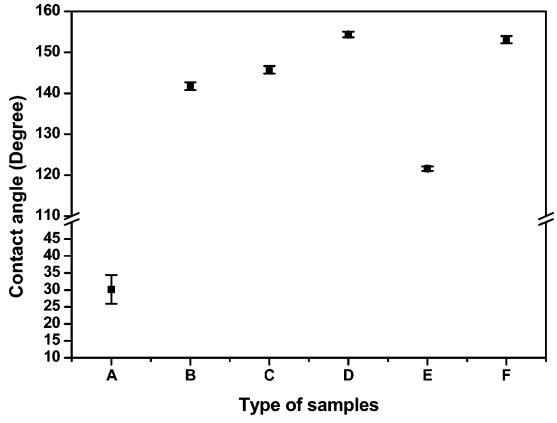

Figure 10. Contact angle of various substrates. The tick labels "A" through "D" represent CNT-grafted-CNFs prepared with $Fe(Acc)_3$ concentration of 0, 1, 2, and 3 wt %, respectively; "E" and "F" represent the carbon paper without and with CNT grafting, respectively.

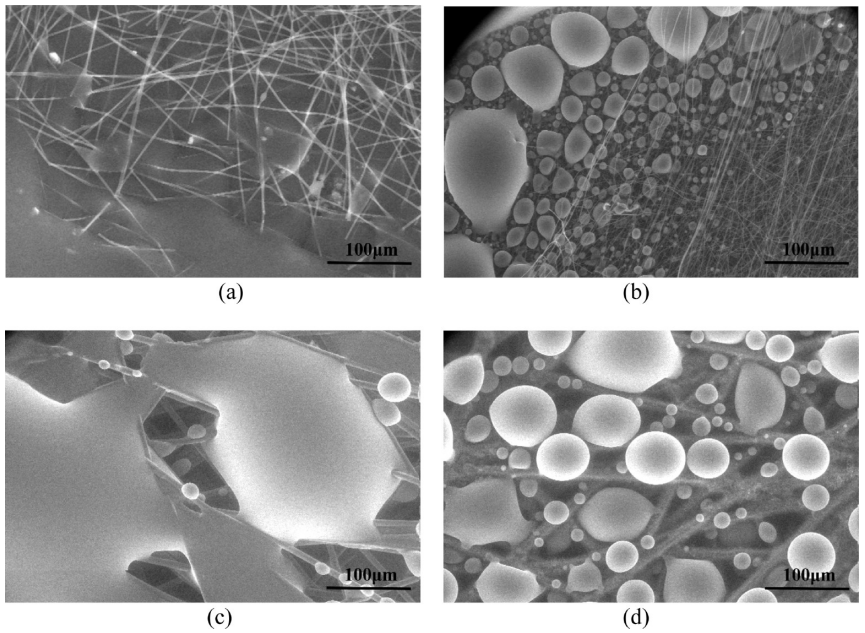

Figure 11. Water condensation behavior on several substrates with different hierarchical surface: (a) CNFs, (b) CNT-grafted-CNFs, (c) carbon paper (consisting of microscale carbon fibers), and (d) CNT-grafted carbon paper.

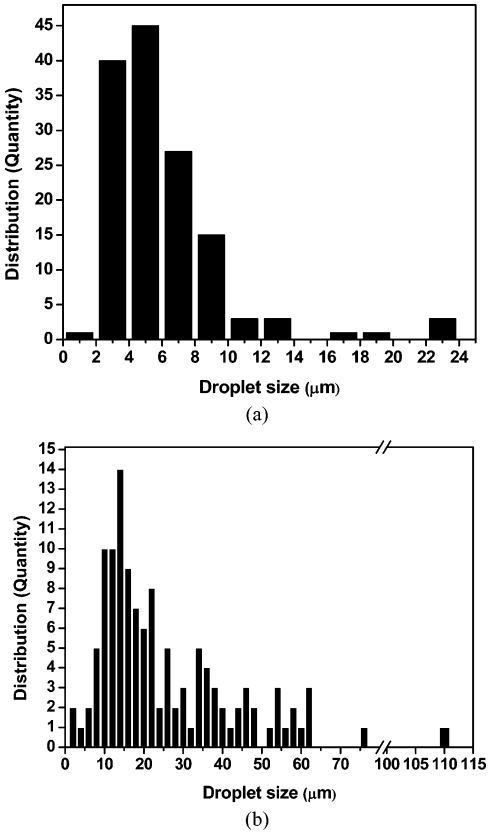

Figure 12. Water droplet size distributions (a) nano/nano CNT-grafted-CNFs and (b) micro/nanoscale CNT-grafted carbon paper.

as the filaments supported them. When a droplet on a filament met another on a neighboring filament, they coalesced into a large droplet without spreading out due to the hydrophobicity of the CNT-grafted carbon paper. This phenomenon occurred in the CNT-grafted-CNFs; however, due to the nanosized filaments (nanofibers), the water droplets were not as large as on CNT-grafted carbon papers. The larger scale of the roughness (determined by the size of the filaments prior to CNT growth) can determine the potential applications of the surface. For applications in water collecting, the CNT-grafted carbon paper (with microscale unevenness on the substrate) is preferable to the CNT-grafted CNFs (with nanoscale unevenness on the substrate) because large droplets can coalesce and be collected efficiently. However, if the application of the substrate is to rapidly dry moisture, the CNT-grafted-CNFs are more desirable because smaller water droplets will evaporate quickly and dry out.

4. CONCLUSION

The effect of the scale of micro/nano hierarchical patterned surfaces was investigated by fabricating CNT-grafted-CNFs and CNT-grafted carbon paper surfaces. The effect of catalysts contained in the electrospinning solution on the microstructure and the size of the resulting CNFs and CNTs were examined, showing that an increase in the amount of catalyst reduced the electrical conductivity of the solution, resulting in thinner nanofibers and thicker CNTs, as well as superhydrophobicity. The large-scale surface roughness of the CNT-grafted-CNFs and the CNT-grafted carbon papers were different. Because of the hierarchical nature of the surfaces, superhydrophobic behavior against large water droplets was observed in both cases. However, the surface behavior of the two samples with small water droplets was different, which is attributable to the difference in the scale of the substrate unevenness. The CNT-grafted-CNF surface, with the nano/nano hierarchical pattern, was more suitable for rapid-drying applications, whereas the CNT-grafted paper was more suited to water-collection applications because only large water droplets were supported, leading to coalescence.

AUTHOR INFORMATION

Corresponding Author

*Tel.: +82 2 880 9096. Fax: +82 2 883 8197. E-mail address: woongryu@anu.ac.kr.

Notes

The authors declare no competing financial interest.

■ ACKNOWLEDGMENTS

This work was supported by DAPA and ADD and by a grant from the Korea Science and Engineering Foundation (KOSEF) funded by the Korean government (MEST) (R11-2005-065) through the Intelligent Textile System Research Center (ITRC).

■ REFERENCES

(1) Lapshin, R.; Alekhin, A.; Kirilenko, A.; Odintsov, S.; Krotkov, V. *J. Surf. Invest.: X-ray, Synchrotron Neutron Techn.* **2010**, *4*, 1−11.
(2) Alekhin, A.; Boleiko, G.; Gudkova, S.; Markeev, A.; Sigarev, A.; Toknova, V.; Kirilenko, A.; Lapshin, R.; Kozlov, E.; Tetyukhin, D. *Nanotechnol. Russia* **2010**, *5*, 696−708.
(3) Bertazzo, S.; Rezwan, K. *Langmuir* **2009**, *26*, 3364−3371.
(4) Zhang, W.; Wahlgren, M.; Sivik, B. *Desalination* **1989**, *72*, 263−273.
(5) Ikada, Y. *Biomaterials* **1994**, *15*, 725−736.
(6) Stein, A.; Melde, B. J.; Schroden, R. C. *Adv. Mater.* **2000**, *12*, 1403−1419.
(7) Cao, L.; Jones, A. K.; Sikka, V. K.; Wu, J.; Gao, D. *Langmuir* **2009**, *25*, 12444−12448.
(8) Jung, Y. C.; Bhushan, B. *ACS Nano* **2009**, *3*, 4155−4163.
(9) Tu, C.-W.; Tsai, C.-H.; Wang, C.-F.; Kuo, S.-W.; Chang, F.-C. *Macromol. Rapid Commun.* **2007**, *28*, 2262−2266.
(10) Pei, M.-D.; Wang, B.; Li, E.; Zhang, X.-h.; Song, X.-m.; Yan, H. *Appl. Surf. Sci.* **2010**, *256*, 5824−5827.
(11) Barthlott, W.; Neinhuis, C. *Planta* **1997**, *202*, 1−8.
(12) Liu, K.; Yao, X.; Jiang, L. *Chem. Soc. Rev.* **2010**, *39*, 3240−3255.
(13) Guo, Z.; Liu, W.; Su, B.-L. *J. Colloid Interface Sci.* **2011**, *353*, 335−355.
(14) Clark, D. T.; Feast, W. J.; Musgrave, W. K. R.; Ritchie, I. *J. Polym. Sci.: Polym. Chem. Ed.* **1975**, *13*, 857−890.
(15) Hopkins, J.; Badyal, J. P. S. *J. Phys. Chem.* **1995**, *99*, 4261−4264.
(16) Ryan, M. E.; Fonseca, J. L. C.; Tasker, S.; Badyal, J. P. S. *J. Phys. Chem.* **1995**, *99*, 7060−7064.
(17) Lau, K. K. S.; Bico, J.; Teo, K. B. K.; Chhowalla, M.; Amaratunga, G. A. J.; Milne, W. I.; McKinley, G. H.; Gleason, K. K. *Nano Lett.* **2003**, *3*, 1701−1705.
(18) Liu, H.; Feng, L.; Zhai, J.; Jiang, L.; Zhu, D. *Langmuir* **2004**, *20*, 5659−5661.
(19) Shirtcliffe, N. J.; McHale, G.; Newton, M. I.; Perry, C. C. *Langmuir* **2003**, *19*, 5626−5631.
(20) Jiang, L.; Zhao, Y.; Zhai, J. *Angew. Chem., Int. Ed.* **2004**, *43*, 4338−4341.
(21) Ma, M.; Hill, R. M.; Lowery, J. L.; Fridrikh, S. V.; Rutledge, G. C. *Langmuir* **2005**, *21*, 5549−5554.
(22) Zhang, G.; Wang, D.; Gu, Z.-Z.; Möhwald, H. *Langmuir* **2005**, *21*, 9143−9148.
(23) Shi, F.; Liu, Z.; Wu, G. L.; Zhang, M.; Chen, H.; Wang, Z. Q.; Zhang, X.; Willner, I. *Adv. Funct. Mater.* **2007**, *17*, 1821−1827.
(24) Nakanishi, T.; Michinobu, T.; Yoshida, K.; Shirahata, N.; Ariga, K.; Möhwald, H.; Kurth, D. G. *Adv. Mater.* **2008**, *20*, 443−446.
(25) Nakanishi, T.; Shen, Y.; Wang, J.; Li, H.; Fernandes, P.; Yoshida, K.; Yagai, S.; Takeuchi, M.; Ariga, K.; Kurth, D. G.; Mohwald, H. *J. Mater. Chem.* **2010**, *20*, 1253−1260.
(26) Öner, D.; McCarthy, T. J. *Langmuir* **2000**, *16*, 7777−7782.
(27) Li, H.; Wang, X.; Song, Y.; Liu, Y.; Li, Q.; Jiang, L.; Zhu, D. *Angew. Chem., Int. Ed.* **2001**, *40*, 1743−1746.
(28) Huang, L.; Lau, S. P.; Yang, H. Y.; Leong, E. S. P.; Yu, S. F.; Prawer, S. *J. Phys. Chem. B* **2005**, *109*, 7746−7748.
(29) Hsieh, C.-T.; Chen, W.-Y.; Wu, F.-L. *Carbon* **2008**, *46*, 1218−1224.
(30) Hikita, M.; Tanaka, K.; Nakamura, T.; Kajiyama, T.; Takahara, A. *Langmuir* **2005**, *21*, 7299−7302.
(31) Shirtcliffe, N. J.; McHale, G.; Newton, M. I.; Chabrol, G.; Perry, C. C. *Adv. Mater.* **2004**, *16*, 1929−1932.
(32) Hsieh, C.-T.; Chen, W.-Y.; Wu, F.-L.; Hung, W.-M. *Diamond Relat. Mater.* **2010**, *19*, 26−30.
(33) Fürstner, R.; Barthlott, W.; Neinhuis, C.; Walzel, P. *Langmuir* **2005**, *21*, 956−961.
(34) Jang, J.; Bae, J.; Park, E. *Adv. Funct. Mater.* **2006**, *16*, 1400−1406.
(35) Peter K, B. *J. Colloid Interface Sci.* **1971**, *36*, 71−79.
(36) Ko, F.; Gogotsi, Y.; Ali, A.; Naguib, N.; Ye, H.; Yang, G. L.; Li, C.; Willis, P. *Adv. Mater.* **2003**, *15*, 1161−1165.
(37) Wang, L.; Yu, Y.; Chen, P. C.; Zhang, D. W.; Chen, C. H. *J. Power Sources* **2008**, *183*, 717−723.
(38) Ōya, A.; Marsh, H. *J. Mater. Sci.* **1982**, *17*, 309−322.
(39) Shinn-Shyong, T. *Carbon* **2006**, *44*, 1986−1993.
(40) Ko, T.-H.; Liao, Y.-K.; Liu, C.-H. *New Carbon Mater.* **2007**, *22*, 97−101.
(41) Reneker, D. H.; Yarin, A. L. *Polymer* **2008**, *49*, 2387−2425.
(42) Terrones, H.; Hayashi, T.; Muñoz-Navia, M.; Terrones, M.; Kim, Y. A.; Grobert, N.; Kamalakaran, R.; Dorantes-Dávila, J.; Escudero, R.; Dresselhaus, M. S.; Endo, M. *Chem. Phys. Lett.* **2001**, *343*, 241−250.
(43) Krishnan, A.; Dujardin, E.; Treacy, M. M. J.; Hugdahl, J.; Lynum, S.; Ebbesen, T. W. *Nature* **1997**, *388*, 451−454.
(44) Maiti, A.; Brabec, C. J.; Bernholc, J. *Phys. Rev. B* **1997**, *55*, R6097−R6100.
(45) Kim, K. J.; Yu, W.-R.; Youk, J. H.; Lee, J. *Phys. Chem. Chem. Phys.* **2012**, *14*, 14041−14048.
(46) Cortese, B.; D'Amone, S.; Manca, M.; Viola, I.; Cingolani, R.; Gigli, G. *Langmuir* **2008**, *24*, 2712−2718.